A Simple Method for MR Elastography: A Gradient-Echo Type Multi-Echo Sequence

Tomokazu Numano[1,4], Kazuyuki Mizuhara[2], Junichi Hata[1,3], Toshikatsu Washio[4], Kazuhiro Homma[4]

[1]Department of Radiological Science, Graduate School of Human Health Science, Tokyo Metropolitan University
7-2-10, Higashiogu, Arakawa-ku, Tokyo, Japan
TEL +81-3-3819-1211
FAX +81-3-3819-1406
e-mail: t-numano@tmu.ac.jp

[2]Department of Mechanical Engineering, TOKYO DENKI UNIVERSITY

[3]The University of Tokyo Hospital

[4]Human Technology Research Institute, National Institute of Advanced Industrial Science and Technology (AIST)

Abstract

To demonstrate the feasibility of a novel MR Elastography (MRE) technique based on a conventional gradient-echo type multi-echo MR sequence which does not need additional bipolar magnetic field gradients (motion encoding gradient: MEG), yet is sensitive to vibration. In a gradient-echo type multi-echo MR sequence, several images are produced from each echo of the train with different echo times (TEs). If these echoes are synchronized with the vibration, each readout's gradient lobes achieve an MEG-like effect and the later generated echo causes a greater MEG-like effect. The sequence was tested for the tissue-mimicking agarose gel phantoms and the psoas major muscles of healthy volunteers. It was confirmed that the readout gradient lobes caused an MEG-like effect and the later TE images had higher sensitivity to vibrations. The magnitude image of later generated echo suffered the T2 decay and the susceptibility artifacts, but the wave image and elastogram of later generated echo were unaffected by these effects. In in vivo experiments, this method was able to measure the mean shear modulus of the psoas major muscle. From the results of phantom experiments and volunteer studies, it was shown that this method has clinical application potential.

Key Words: MR Elastography; multi-echo sequence; motion encoding gradient; pneumatic vibration; synchronization; psoas major muscle

1. Introduction

It is well known that many pathologies cause changes in tissue elasticity, and tissue palpation is one of the most fundamental diagnostic tools employed by physicians. However, palpation is subjective and not all tissues are accessible to the physician's probing, for example, it is virtually impossible to palpate deeper tissues. With that in mind, several qualitative and quantitative methods to evaluate the elasticity of tissues have been proposed as diagnostic tools for detection of abnormal stiffness in soft tissues. Among them, ultrasound-based and magnetic resonance imaging (MRI) -based elastogram techniques are the most used methods. An MRI-based elastogram technique, MR Elastography (MRE), is a relatively new technique which allows the measurement of mechanical properties such as the shear moduli of biological tissues and materials. There are two principally different methods of MRE: static [1] and dynamic [2-5]. Static MRE uses two different static compressional states of the investigated material to determine its corresponding distortions. Dynamic MRE is the mainstream of MRE in in vivo applications such as brain [5-9], breast [5,10,11], liver [5,12-14], prostate [15,16], and muscle [5,17,18]. The cyclic shear motions synchronized with the MR pulse sequence are applied to the tissue of interest by using external vibration sources, and the resultant oscillating displacements are embedded into the MR phase images by using bipolar gradient lobes (motion-encoding gradient: MEG) inserted into conventional MR pulse sequences [2,5]. The cyclic

shear motions were frequently used by separated oscillations (burst oscillations) in each excitation/acquisition. When the period of external vibration and MEG are in agreement, MEG has the maximum effect. In short, the implementation of MEG increases the sensitivity of the MRE pulse sequence to the vibration. The recorded wave images (MR phase images) are converted into shear stiffness image (elastogram) by using an inversion algorithm. The local frequency estimate (LFE) algorithm has been used routinely as an inversion algorithm [19]. The strength of a propagation wave was attenuated according to the depth from surface. In deeper tissue, low-strength of a propagating wave, the MR phase shift is decreased and it becomes difficult to detect the vibrations. It is possible to increase the sensitivity by increasing repetition of MEG. Since the MEG is placed in between the radiofrequency (RF) excitation pulse and the echo signal, it prolongs the TE. Thus, increasing the MEG further prolongs the TE, which tends to reduce the signal to noise ratio (SNR) of the MR signal, and increases the magnetic susceptibility effects.

We propose a simple MRE method that does not need a built-in MEG (no prolongation of TE). A gradient-echo type multi-echo imaging sequence use a series of echoes acquired as a train following after a single excitation pulse. Multiple symmetrical gradient-echoes are acquired by the symmetrical bipolar readout gradient lobes. The readout gradient lobes have a similar function to MEG (MEG-like effect). Subsequently, if those gradient lobes are synchronized with vibrations, they work as MEGs. This synchronization can be easily achieved by adjusting the period of bipolar readout gradient lobes and the gap between the first and next echo (δTE) of a multi-echo sequence. If the δTE is synchronized with the vibration frequency, the later generated echo has a greater MEG-like effect (1st echo < 2nd echo < 3rd echo, etc.). Consequently, a multi-echo sequence acquires images with different MEG weightings and echo times without increasing the acquisition time. The proposed MRE experimental design was employing continuous (steady state) vibrations throughout the whole acquisition. Therefore, the frequency of vibrations is needed synchronizing on the repetition time (TR). The purpose of this study was to test the MEG-less multi-echo MRE method using a clinical MR imager, and to examine the character of this method by the tissue-mimicking agarose gel phantoms. In addition, we conducted volunteer studies on psoas major muscles by using the MEG-less multi-echo MRE.

2. Materials and methods

2.1 MEG-less Multi-echo MRE Sequence

Fig. 1 shows a MEG-less multi-echo MRE sequence. The MEG-less multi-echo MRE sequence takes advantage of a gradient-echo type multi-echo MR sequence to obtain an MR elastogram. A gradient-echo type multi-echo MR sequence uses a series of echoes acquired as a train following a single excitation RF pulse. Multiple symmetrical gradient-echoes can be acquired by the symmetrical bipolar readout gradient lobes. A gradient-echo type multi-echo MR sequence has two

benefits. Major benefit, the multiple gradient-echoes is useful to reduce the acquisition time of MRI or MRE [20]. Second benefit, a multi-echo MR sequence acquires images with different weightings and / or TEs and is used to obtain various images without increasing the acquisition time. The MEG-less multi-echo MRE sequence uses of the second benefit. By adjusting the period of bipolar readout gradient lobes, the TE-interval (δTE; Fig. 1 arrowed dash line) of a multi-echo MR sequence can be changed. Thus, the frequency of actuator-generated vibration and the readout gradient lobes were matched exactly. The readout gradient lobes have a similar function to MEG (MEG-like effect). When the period of actuator-generated vibration and the readout gradient lobes are the same (Fig. 1 dash line), the MEG-like effect is maximal. Moreover, since the later generated echo experienced a greater MEG-like effect (1st < 2nd < 3rd, etc.), then the MEG-less MRE multi-echo sequence acquires images with different MEG-like effects without increasing the acquisition time. In other words, the user can choose from different MEG-like weighted images after MR scans. If the maximal MEG-like effect is not required, it is not necessary to match the actuator-generated vibration frequency and the δTE. The reason for this is that if the phase of each pixel is sampled for several relative phases between the displacements (displacements of vibration) and the MEG, the amplitude and phase of the displacements may be found uniquely via the Fourier transformation of the phases for each voxel. Trigonometry can be used to show that the integral of an arbitrary signal and a sinusoid is a sinusoidal function of the phase between the two. Therefore, practically any gradient waveform can be used to encode displacement and the methods currently used to provide the amplitude and phase of the induced vibrations can be applied directly [21]. However, unlike the real MEG, the MEG-like effect is not tuned for a specific vibration frequency and has sensitivity to a wider range of frequencies. The selective detection of the applied vibration frequency was achieved by adjusting the TR of a MEG-less multiecho MRE sequence, and the TR must be multiple of vibration period. In other words, in this method, the vibration frequency is set to an integer multiple of 1/TR, and the vibration period does not necessarily match the δTE.

2.2 MRE experiments

All MRI and MRE experiments were performed on a clinical MR imager (Achieva 3.0T; Philips Healthcare, Best, The Netherlands). A self-made waveform generation system (LabVIEW, USB-6221; National Instruments, TX, USA) was used to generate the vibration waveform. In order to synchronize the vibration with TR, the transistor-transistor logic (TTL) signal form the MRI system (RF pulse power amplifier) was used as a trigger the start of the vibration. This system is capable of generating sinusoidal waveforms with arbitrary frequencies and phases. In this MRE system, the vibration phase offset was controlled by the waveform generator, giving continuous (steady state) vibrations throughout the whole acquisition (each imaging period). Power amplifier (XTi 1000; Crown, IN, USA) and a pneumatic pressure generator (Subwoofer TIT320C-4 12”;

Dayton Audio, OH, USA) units were used to supply vibrations to a vibration pad. We designed some vibration pads of suitable forms for each imaging object by using a 3D printer (3DTouch; 3D Systems, SC, USA). All MRE image processing was performed by Local Frequency Estimate (LFE) algorithm freeware (MRE/Wave, MAYO CLINIC).

2.3 Phantom experiments

The phantom MRE experiments were conducted by the use of four types of tissue-mimicking phantom. The tissue-mimicking phantom compositions are listed in Table 1. A gadolinium contrast agent (Gadoteridol; Bracco-Eisai, Tokyo, Japan) was varied T2 value and a 10 mmΦ zirconia ball (YTZ ball; Nikkato, Osaka, Japan) was generated of magnetic susceptibility effects in the phantom. All phantoms were prepared in a 2.0 liter cylindrical rigid vinyl chloride container with a diameter of 155 mm. A higher agarose gel concentration (3.0 wt%) layer was used to protect the each phantom's surface (Fig. 2a). We conducted phantom MRE experiments at 100 Hz vibration, and it was synchronized with 5 ms of δTE. We validated the character of a MEG-less multi-echo MRE sequence by through the phantom experiments. Additionally we compared differences in wave images to assess the differences in frequency encoding (readout) direction. All wave images was processed by a phase unwrapping and a spatial frequency bandpass filter (isochromat oscillation cycles / FOV). For all phantom MRE experiments, imaging parameters were kept constant, except for the readout direction. The phantom experiments' MEG-less multi-echo MRE sequence imaging parameters are listed in Table 2. The T2 value of the phantoms was measured with a long-TR spin-echo type multi-echo sequence with different TE images. 8-element phased array coil (SENSE head coil; Philips Healthcare, Best, The Netherlands) was used for all phantom experiments.

2.4 Volunteer studies

The psoas major muscle of three healthy young male volunteers was examined with MRE using a 50 Hz vibration frequency. The penetrating power of a low vibration frequency (50 Hz) is greater than a high vibration frequency (100 Hz). We have selected 50 Hz, in order to reach a vibration of sufficient amount at the psoas major muscle. For mechanical excitation of the muscle tissue, a couple of vibration pads were placed on the lumbar area of prone posture (Fig.6b). For acquisition parameters, see Table 2. Volunteers did breath-holding during each MRE acquisition (20.5 sec). 6-element phased array coil (SENSE torso coil; Philips Healthcare, Best, The Netherlands) was used for all volunteer studies. All volunteer studies were done after obtaining informed consent from all volunteers and being approved by our institutional Ethical Review Board.

3. Results

3.1 Phantom experiments

Fig. 2b-h shows the unwrapped MR phase images (wave images) of each echo and demonstrate the MEG-like effect in the middle T2 (P1) phantom. Fig. 2i shows the fast Fourier transform results of the profile data, through white lines of each wave images The period of the readout gradient (Fig. 1 dash line) is twice the period of δTE (Fig. 1 arrowed dash line). Therefore, setting the δTE to 5.0 ms resulted in a period readout gradient of 10 ms, matching a 100 Hz vibration frequency. Because the δTE (5.0 ms) was synchronized with vibration frequency (100 Hz), the later generated echo experienced showed a greater MEG-like effect.

Fig. 3a demonstrates the change in the relative signal intensity of the magnitude images and the relative phase shift of the wave images, vs. the echoes (TEs) on each T2 (P1, P2, P3) phantom, normalized with those of the 1st echo. The signal intensity decreasing rate of each phantom was depended on the T2 of phantom. On the other hand, for the relative phase shift, there was no correlation between the T2 of phantom. The MEG-like effect (increase rate of the relative phase shift) of each phantom was proportional to the number of echoes. Fig. 3b demonstrates the phantom stiffness vs. the TEs on each phantom. The phantom stiffness of the TEs was approximately-constant value on each phantom. This result shows that, there was no correlation between the phantom stiffness and the T2 of phantom.

Fig. 4 shows the influence of magnetic susceptibility in the susceptibility (P4) phantom. The later TE suffered magnetic susceptibility artifacts on the magnitude image. On the other hand, the wave image of the later TE seems unaffected by the magnitude susceptibility, and the elastogram of the later TE was free of the influence of magnetic susceptibility effect.

Fig. 5 demonstrates the P1 phantom wave images and the elastograms with the choice of the frequency encoding (readout) direction. The images were acquired in coronal orientation. Shown is the 3rd echo, for example. Because the MEG-less multi-echo MRE sequence has vibration sensitivity in the readout direction, the pattern of the wave image was changed by choosing the readout direction. In the case of the L-R readout direction (Fig. 5c), the pattern of wave image was like a chessboard. In the case of the H-F readout direction (Fig. 5e), the pattern of the wave image was bilaterally symmetric. The elasticity reconstruction yielded a mean shear moduli of 6.75 ± 0.91 kPa for the L-R readout direction and 6.22 ± 1.02 kPa for the H-F readout direction in the P1 phantom, including the standard deviation (SD) of the values inside the region of interest (ROI). These mean shear moduli give close agreement with literature values [7].

3.2 Volunteer studies

Fig. 6 demonstrates the wave images (c,e) and elastograms (d,f) obtained from different echoes in volunteer psoas major muscles, respectively. These images were magnitude images (Fig. 6a) overlaid with the wave image or elastogram. Fig. 6b shows the position of vibration pads and the ROIs of psoas major muscles. As in the case of agarose phantom experiments, the sensitivity to the vibration

increased in later TE. This was effective for detecting waves in deeper tissues where vibrations were weak. Wave passing through the psoas major muscles was spread like ripples from the lumbar spine. It would appear that because the psoas major muscles are attached to the lumbar spine, the vibration of the lumbar spine transferred vibrations efficiently to the psoas major muscles. The mean shear modulus listed in Table 3. The different echoes showed only a small variance in the mean shear modulus value.

4. Discussion

The results demonstrate that the MEG-less multi-echo MRE sequence enables to acquire elastograms of both tissue-mimicking agarose gel phantoms and volunteer muscles. In this sequence, each symmetrical bipolar readout gradient lobe increases the vibration sensitivity. In addition, the multi-echo sequence acquires images with different TEs and / or vibration weightings without increasing the acquisition time. From this unique feature, the user can choose an appropriate image from different MEG-like weighted images after the MR scans. The magnitude image of the 1st echo has the smallest MR phase shifts, but provides the best anatomical structure images because the 1st echo has the highest signal to noise ratio (SNR), and it is less affected by magnetic susceptibility artifacts. As a result, the magnitude image of the 1st echo is useful to make structures and elastogram fusion images (Fig. 6), while it does not require position adjustment or image compensation. Moreover, this method demonstrated that MRE can be performed by using a common gradient echo type multi-echo sequence, and a dedicated MRE sequence (built-in MEG) is not always necessary for MRE. During the phantom experiment, when the δTE matches the vibration frequency, the phase shift accumulation behavior of the MEG-like effect was found not to depend on both the influence of T2 and the influence of magnetic susceptibility of the imaging object. These results demonstrate the robustness of the MR phase shift information under the effect of magnetic susceptibility effect and the lower SNR condition. By signal averaging of each TE elastogram, the MEG-less multi-echo MRE sequence has the potential of improve of the SNR of the elastogram, without adding scan.

Although the MEG-less multi-echo MRE sequence is a very promising technique, its limitations should also be addressed. First, the MEG-less multi-echo MRE sequence is inadequate for an accurate analysis of propagating shear waves. In All MRE sequence, vibration displacement only in the same direction as a bipolar gradient (MEG) will result in a MR phase shift. Therefore, it is necessary to measure all the motion-encoding axes for accurate directional analysis of shear wave propagation. In a dedicated MRE sequence (built-in MEG), it is possible to apply the MEG in any direction regardless of the imaging plane because the MEG is independent of the imaging gradient (phase encoding or frequency encoding etc.). In the MEG-less multi-echo MRE sequence, however, the readout gradient performs as the MEG. Therefore, the motion-encoding direction depends on the readout gradient direction, and it is impossible to detect the vibration in a direction perpendicular to

imaging plane. Specifically, in the coronal imaging plane (Fig. 4a), the MEG-less multi-echo MRE sequence has a motion-encoding effect in the L-R readout direction or H-F readout direction at right angles to each other, but not in the slice direction. The second limitation of the MEG-less multi-echo MRE sequence is that it does not allow multi-frequency vibration MR elastography [22]. Adjustment for multi-frequency vibration setup would be complicated and if at all practically even possible.

The common approach to cancel out MR phase errors in wave images (MR phase images) is to subtract data acquired with the reversed polarity of MEG. In the MEG-less multi-echo MRE sequence, however, the readout gradient performs as the MEG. Therefore, the MEG-less multi-echo MRE sequence was unavailable to the reversed polarity of MEG for the MR phase errors cancellation. The MEG-less multi-echo MRE sequence has other strategy, subtract each opposed phase vibration image (0 vs. π etc.) for the MR phase errors cancellation. Although we have not canceled the MR phase errors in this study, the MR phase errors not have much influence on calculated elastogram. The MR phase errors have influence on the absolute value of phase shift but it has not influence on the wavelength of isochromatic line pattern.

In conclusion, we demonstrated MR Elastography in agarose gel phantom experiments and volunteer psoas major muscle studies by using a conventional gradient-echo type multi-echo MR sequence. The MEG-less multi-echo MRE sequence is a new technique by which several vibration sensitivity images can be obtained from each echo of the train with different TE values. From the results of phantom MRE experiments and volunteer MRE studies, it was shown that the MEG-less multi-echo MRE sequence has clinical application potential.

Acknowledgment

This work was supported in part by a Grant-in-Aid for Scientific Research (25461838) and an Adaptable and Seamless Technology transfer Program (A-STEP AS242Z01253P).

References

1. Plewes DB, Betty I, Urchuk SN, Soutar I. Visualizing tissue compliance with MR imaging. J Magn Reson Imaging 1995;5(6):733-8.
2. Muthupillai R, Lomas DJ, Rossman PJ, Greenleaf JF, Manduca A, Ehman RL. Magnetic resonance elastography by direct visualization of propagating acoustic strain waves. Science 1995;269(5232):1854-7.
3. Muthupillai R, Ehman RL. Magnetic resonance elastography. Nat Med 1996;2(5):601-3.
4. Muthupillai R, Rossman PJ, Lomas DJ, Greenleaf JF, Riederer SJ, Ehman RL. Magnetic resonance imaging of transverse acoustic strain waves. Magn Reson Med 1996;36(2):266-4.
5. Mariappan YK, Glaser KJ, Ehman RL. Magnetic resonance elastography: a review. Clin Anat 2010;23(5):497-511.

6. Johnson CL, McGarry MD, Van Houten EE, et al. Magnetic resonance elastography of the brain using multishot spiral readouts with self-navigated motion correction. Magn Reson Med 2013;70(2):404-12.
7. Latta P, Gruwel ML, Debergue P, Matwiy B, Sboto-Frankenstein UN, Tomanek B. Convertible pneumatic actuator for magnetic resonance elastography of the brain. Magn Reson Imaging 2011;29(1):147-52.
8. Liu GR, Gao PY, Lin Y, et al. Brain magnetic resonance elastography on healthy volunteers: a safety study. Acta Radiol 2009;50(4):423-29.
9. Di Ieva A, Grizzi F, Rognone E, et al. Magnetic resonance elastography: a general overview of its current and future applications in brain imaging. Neurosurg Rev 2010;33(2):137-45
10. Plewes DB, Bishop J, Samani A, Sciarretta J. Visualization and quantification of breast cancer biomechanical properties with magnetic resonance elastography. Phys Med Biol 2000;45(6):1591-610.
11. Sinkus R, Lorenzen J, Schrader D, Lorenzen M, Dargatz M, Holz D. High-resolution tensor MR elastography for breast tumour detection. Phys Med Biol 2000;45(6):1649-64.
12. Rouviere O, Yin M, Dresner MA, et al. MR elastography of the liver: preliminary results. Radiology 2006;240(2):440-8.
13. Venkatesh SK, Yin M, Glockner JF, et al. MR elastography of liver tumors: preliminary results. AJR Am J Roentgenol 2008;190(6):1534-40.
14. Talwalkar JA, Yin M, Fidler JL, Sanderson SO, Kamath PS, Ehman RL. Magnetic resonance imaging of hepatic fibrosis: emerging clinical applications. Hepatology 2008;47(1):332-42.
15. Arani A, Plewes D, Krieger A, Chopra R. The feasibility of endorectal MR elastography for prostate cancer localization. Magn Reson Med 2011;66(6):1649-57.
16. Sahebjavaher RS, Baghani A, Honarvar M, Sinkus R, Salcudean SE. Transperineal prostate MR elastography: initial in vivo results. Magn Reson Med 2013;69(2):411-20.
17. Dresner MA, Rose GH, Rossman PJ, Muthupillai R, Manduca A, Ehman RL. Magnetic resonance elastography of skeletal muscle. J Magn Reson Imaging 2001;13(2):269-76.
18. Bensamoun SF, Ringleb SI, Littrell L, et al. Determination of thigh muscle stiffness using magnetic resonance elastography. J Magn Reson Imaging 2006;23(2):242-7.
19. Manduca A, Oliphant TE, Dresner MA, et al. Magnetic resonance elastography: non-invasive mapping of tissue elasticity. Med Image Anal 2001;5(4):237-54.
20. Maderwald S, Uffmann K, Galban CJ, de Greiff A, Ladd ME. Accelerating MR elastography: a multiecho phase-contrast gradient-echo sequence. J Magn Reson Imaging 2006;23(5):774-80.
21. J. B. Weaver, X. Qin, M. Doyley, E. van Houten, F. Kennedy, Paulsen K. Encoding Harmonic Motion in MR Elastography Using the Imaging Gradients. In: Proceedings of the 11th Annual Meeting of ISMRM, Tronto, 2003 (abstract 1077).

22. Asbach P, Klatt D, Hamhaber U, et al. Assessment of liver viscoelasticity using multifrequency MR elastography. Magn Reson Med 2008;60(2):373-9.

Figure legends

Fig. 1. Sequence diagram for the MEG-less multi-echo MRE sequence. Multiple symmetrical readout gradient lobes generated multiple gradient echoes, and the interval of each gradient echo was δTE (arrowed dashed line). The period of the readout gradient (dashed line) is twice the period of δTE. In this sequence, the vibration was a continuous oscillation, and the vibration frequency required setting to an integer multiple of 1/TR.

Fig. 2. a: Magnitude image acquired in the agarose gel phantom with the 1st echo. The top coat (3.0%) protected the phantom (0.75%) from contact with the vibration pad. b-h: Unwrapped MR phase images (wave images) of each echo. i: The fast Fourier transform results of the profile data, through white lines of each wave image. Because the period of δTE and the vibration frequency are synchronizing, the MEG-like effect (vibration sensitivity enhancement effect) increased with the numbers of generated echo numbers (1st echo < 2nd echo < 3rd, etc.).

Fig. 3. a: Relative signal intensity (normalized with the signal intensity of the 1st echo) and phase shift (normalized with the phase shift of the 1st echo) in the MEG-less multi-echo MRE sequence with echoes (TEs) on each tissue-mimicking T2 (P1, P2, P3) phantom. The value of the relative phase shift is synonymous with the value of the MEG-like effect. The signal intensity decreasing rate of each phantom was depended on the T2 of phantom. On the other hand, there was no correlation between the relative phase shift and the T2 of phantom. b: Phantom stiffness vs. the TEs on each phantom. There was no correlation between the phantom stiffness and the T2 of phantom.

Fig. 4. Influence of magnetic susceptibility in the susceptibility (P4) phantom. The later TE suffered magnetic susceptibility artifacts on the magnitude image. The wave image of the later TE seems unaffected by the magnetic susceptibility, and the elastogram of the later TE shows the same tendency.

Fig. 5. a: Schematic view of the P1 phantom MRE experiment and coronal imaging plane. b: The magnitude image acquired in the phantom with the 1st echo. c,d: The wave image (MR phase image) and an elastogram with the L-R readout direction. e,f: The wave image and the elastogram with an H-F readout direction.

Fig. 6. a: Magnitude image of the lumbar spine with the 1st echo. The volunteer was in the prone

position. b: Schematic of the setup vibration pads and the ROI of the psoas major muscles. c,e: Each image was made by fusion of the wave image with the magnitude image of the 1st echo. d,f: Each image was made by fusion of the elastogram with the magnitude image of the 1st echo.

Table 1 The tissue-mimicking agarose gel phantoms

Tissue-mimicking phantom type	Agarose density [wt %]	Gadoteridol density [mmol/l]	T2 value [ms]	Inclusion
Middle T2: P1	0.75	0	173	-
Short T2: P2	0.75	3.3	37	-
Very Short T2: P3	0.75	6.6	21	-
Susceptibility: P4	0.75	0	173	Zirconia ball 10mmΦ

Table 2 The MEG-less multiecho MRE sequence parameters

Parameter	Phantom	Psoas major muscle
Vibration freq. [Hz]	100	50
Vibration phase offset (radian)	8 (π/4)	8 (π/4)
TR [ms]	40	40
TE of 1st echo [ms]	2.3	2.3
δTE (No. of echoes) [ms]	5.0 (7)	10 (2)
FA [degree]	20	20
Slice thickness [mm]	5	10
FOV [mm^2]	180 × 180	300 × 300 - 320 × 320
Matrix	256 × 256	256 × 256
SENSE [reduction factor]	2.0	2.0
Signal averaging	4	4
Total acquisition time [s]	164	164

FA: flip angle, FOV: field of view, SENSE: sensitivity encoding

Table 3 Mean shear moduli [kPa] of the psoas major muscles including standard deviation of the value inside the ROIs

		1st echo	2nd echo
		Mean ± SD [kPa]	Mean ± SD [kPa]
Volunteer 1	L	1.80 ± 1.04	1.69 ± 0.89
	R	2.33 ± 1.12	2.00 ± 0.72
Volunteer 2	L	1.19 ± 0.40	1.32 ± 0.43
	R	1.17 ± 0.22	1.14 ± 0.26
Volunteer 3	L	2.07 ± 1.06	1.82 ± 0.60
	R	1.30 ± 0.44	1.54 ± 0.25

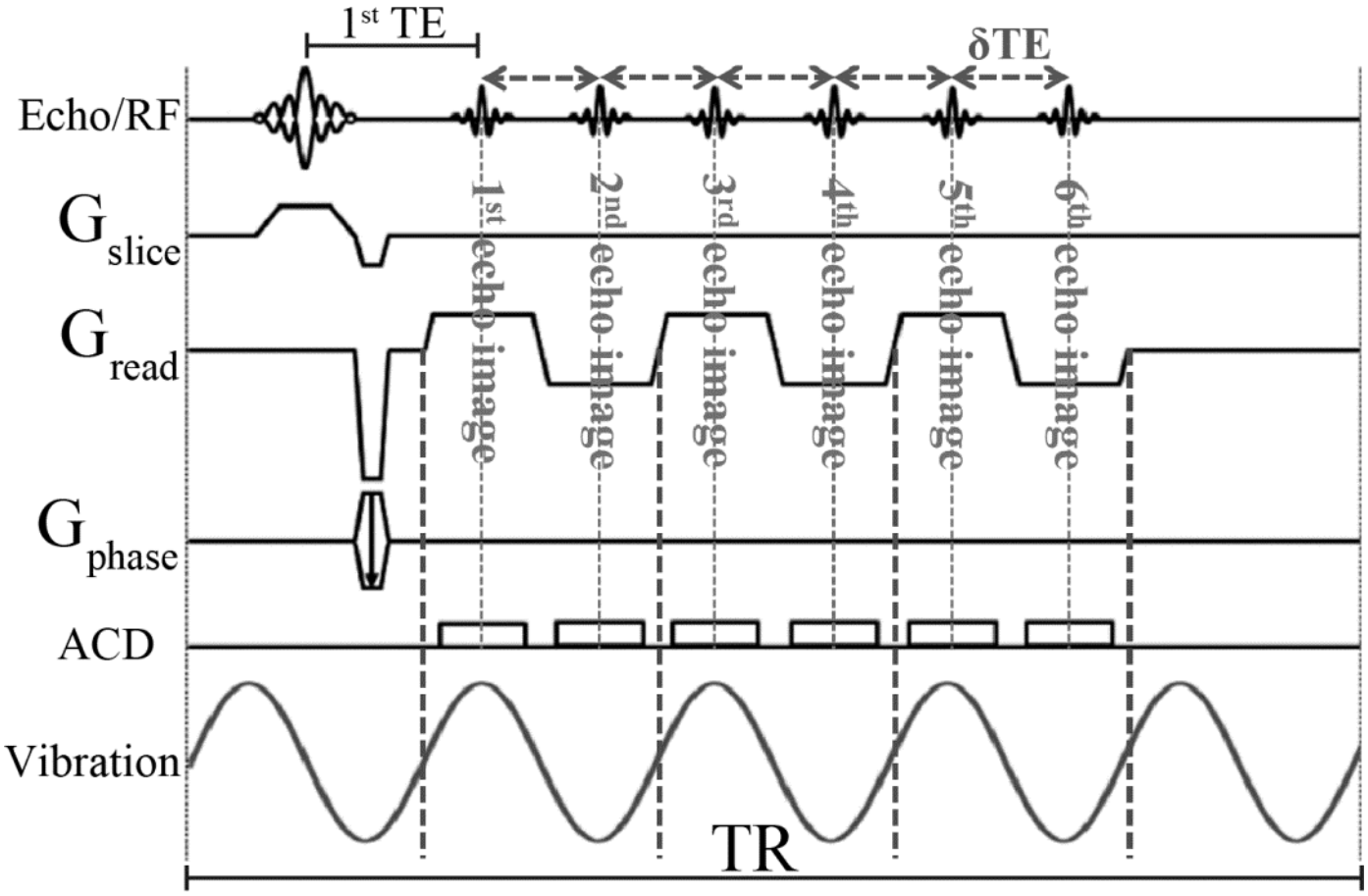
1st TE
δTE
Echo/RF
G slice
G read
G phase
ACD
Vibration
TR
1st echo image
2nd echo image
3rd echo image
4th echo image
5th echo image
6th echo image

Fig.1

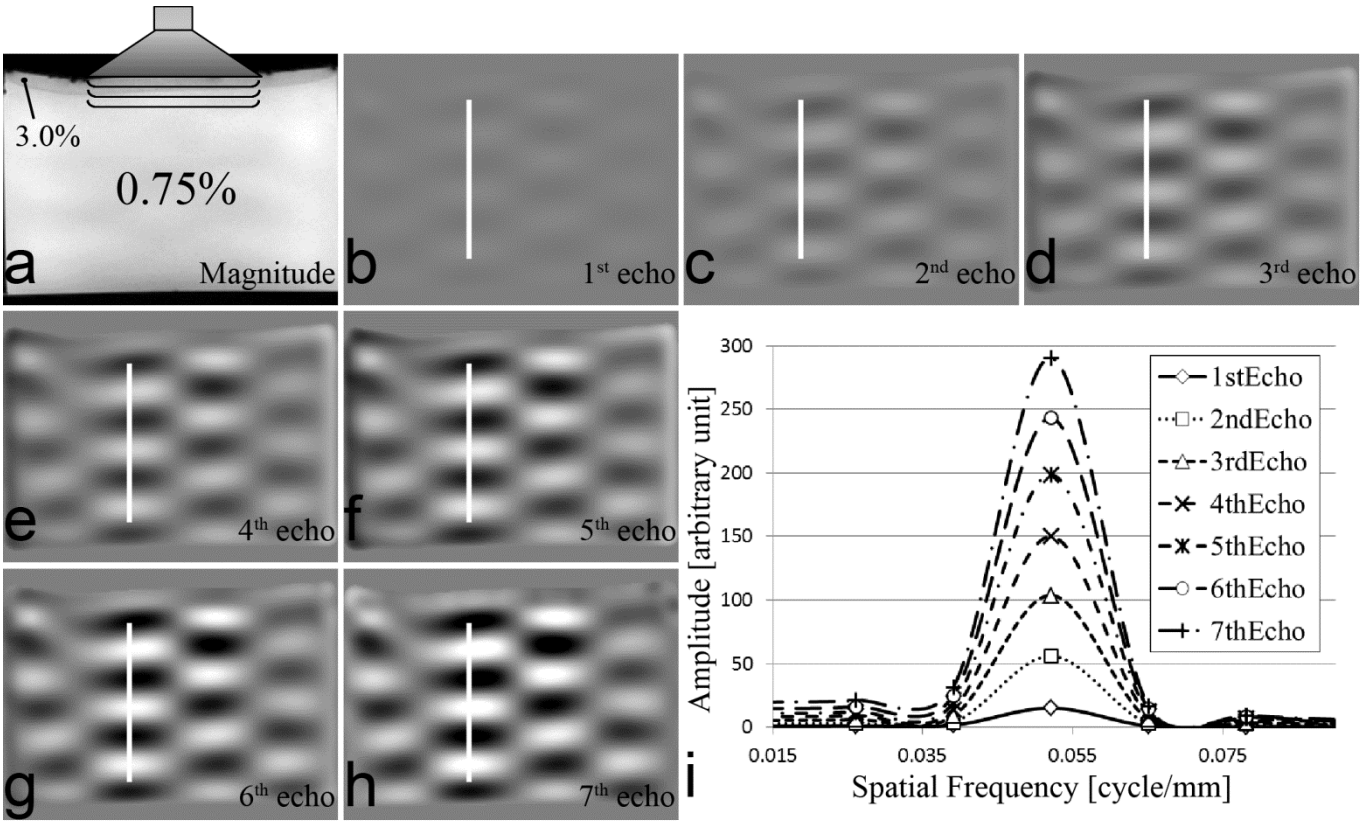
3.0%
0.75%
a Magnitude
b 1st echo
c 2nd echo
d 3rd echo
e 4th echo
f 5th echo
g 6th echo
h 7th echo
i
Amplitude [arbitrary unit]
Spatial Frequency [cycle/mm]
1stEcho
2ndEcho
3rdEcho
4thEcho
5thEcho
6thEcho
7thEcho

Fig.2

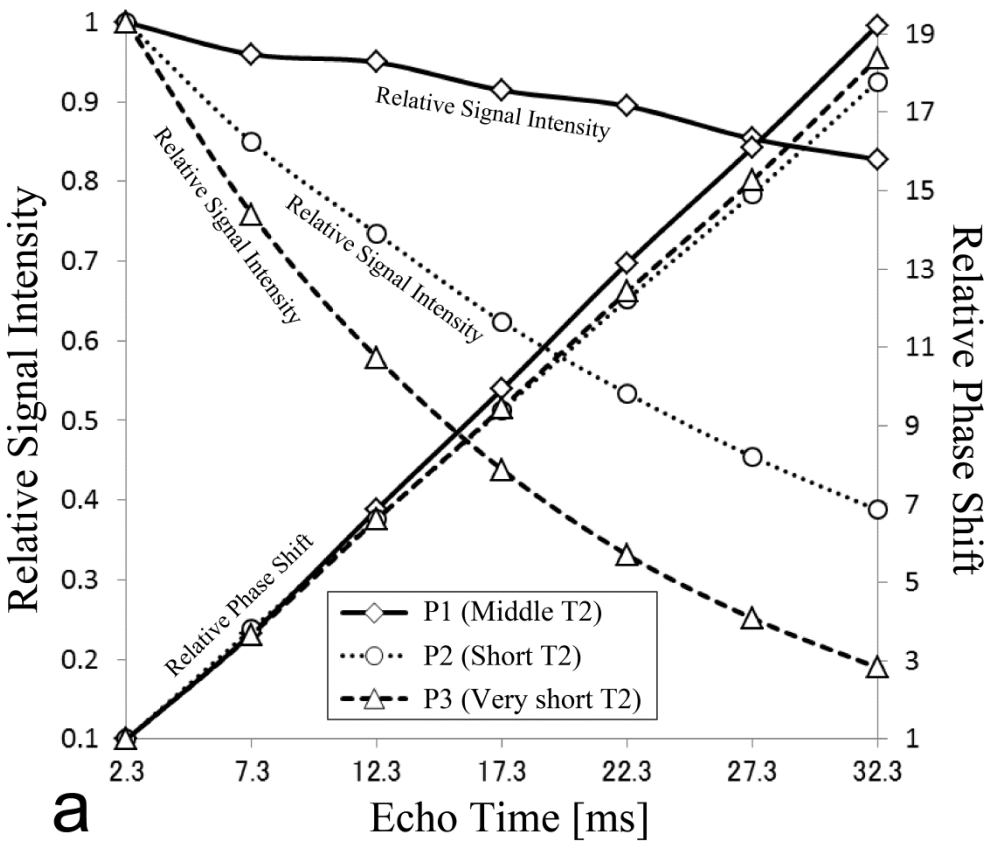
Relative Signal Intensity
Relative Phase Shift
Relative Signal Intensity
Relative Signal Intensity
Relative Signal Intensity
P1 (Middle T2)
P2 (Short T2)
P3 (Very short T2)
Relative Signal Intensity
Relative Phase Shift
Echo Time [ms]
a

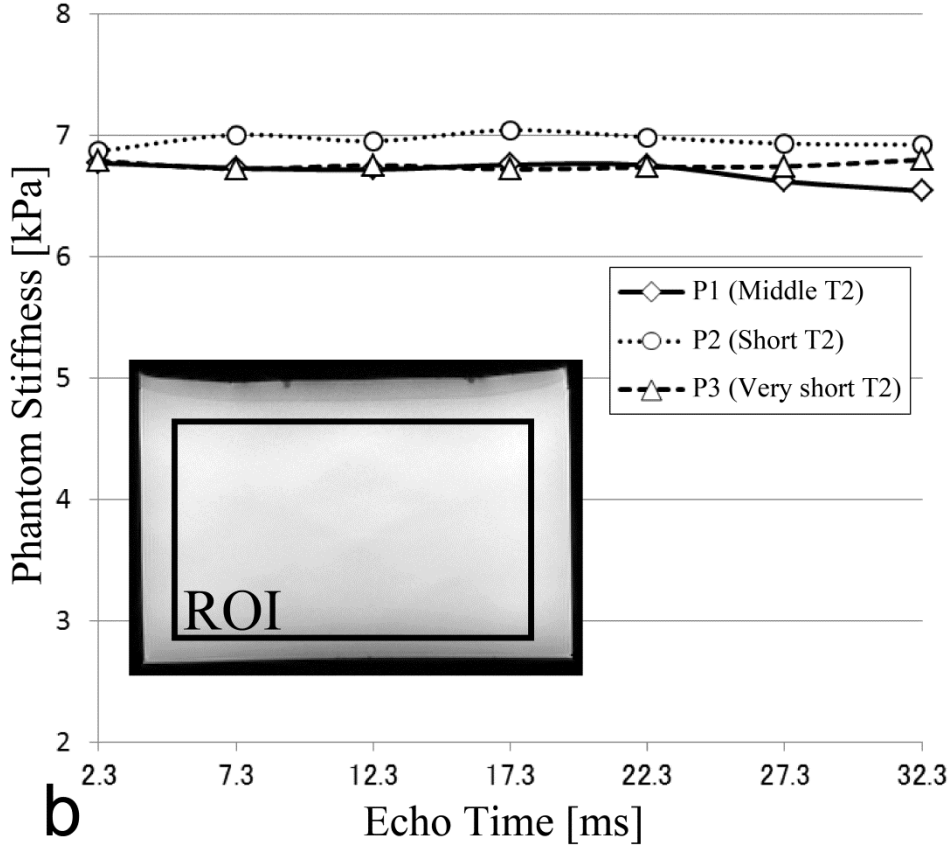
Phantom Stiffness [kPa]
P1 (Middle T2)
P2 (Short T2)
P3 (Very short T2)
ROI
Echo Time [ms]
b

Fig.3

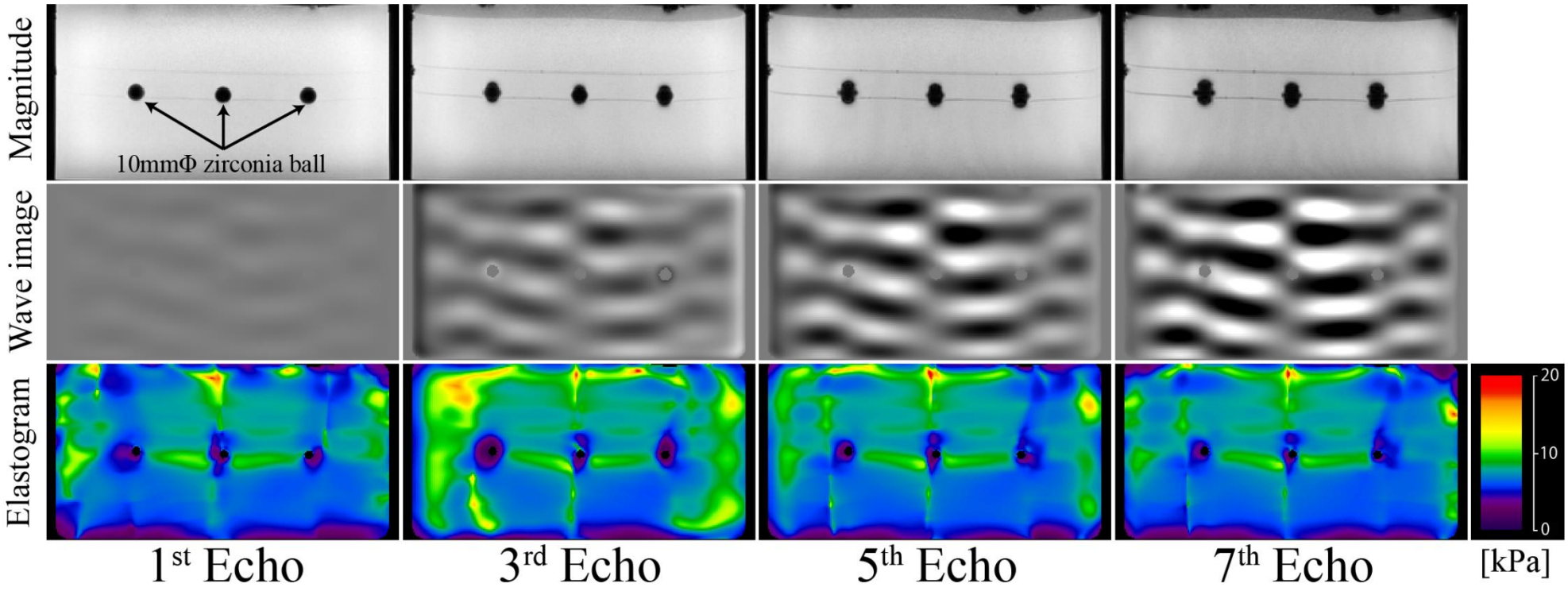
Magnitude
Wave image
Elastogram
10mmΦ zirconia ball
20
10
0
[kPa]
1st Echo
3rd Echo
5th Echo
7th Echo

Fig.4

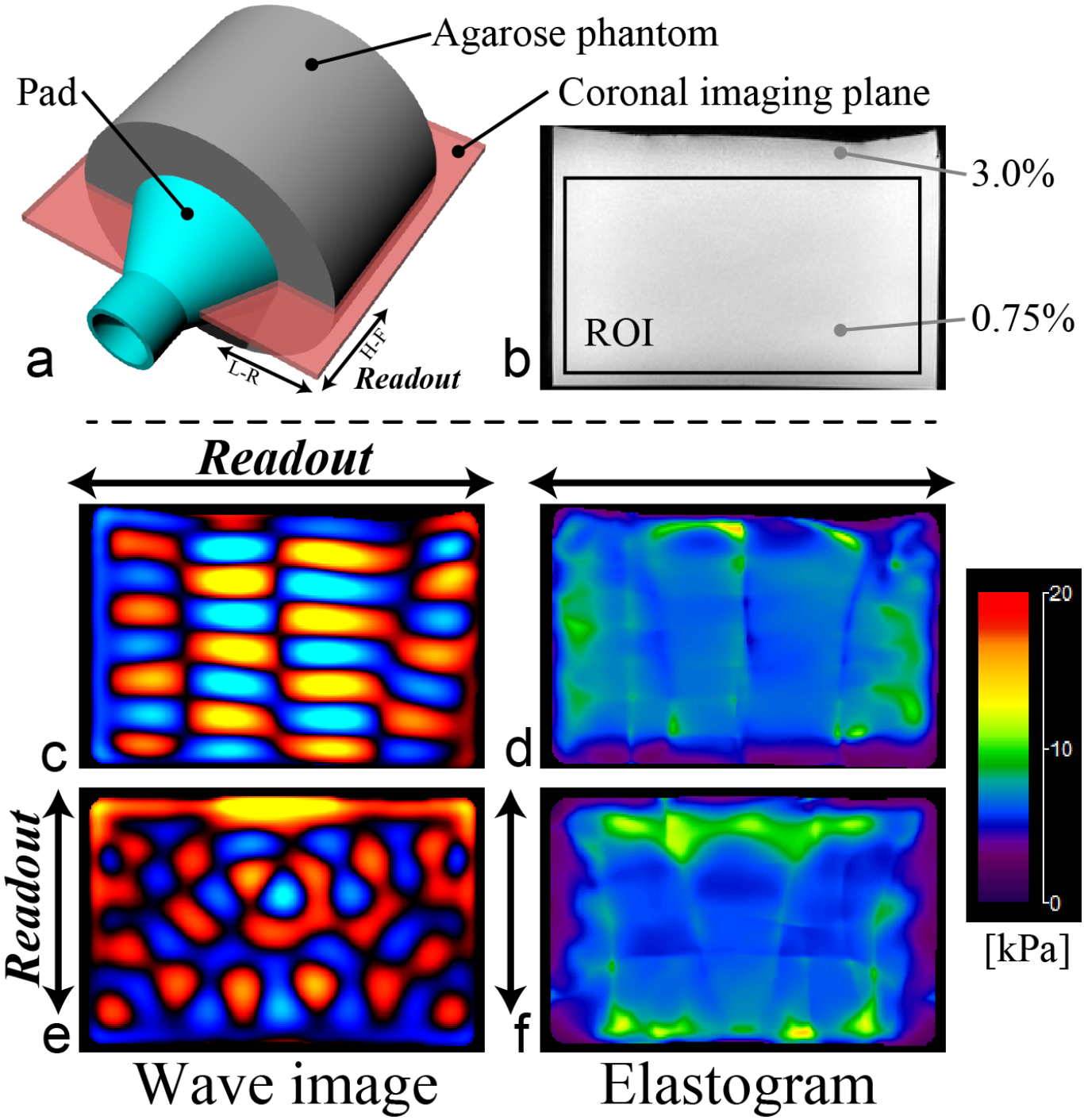
Agarose phantom
Pad
Coronal imaging plane
a
L-R
H-F
Readout
b
ROI
3.0%
0.75%
Readout
c
d
Readout
e
f
20
10
0
[kPa]
Wave image
Elastogram

Fig.5

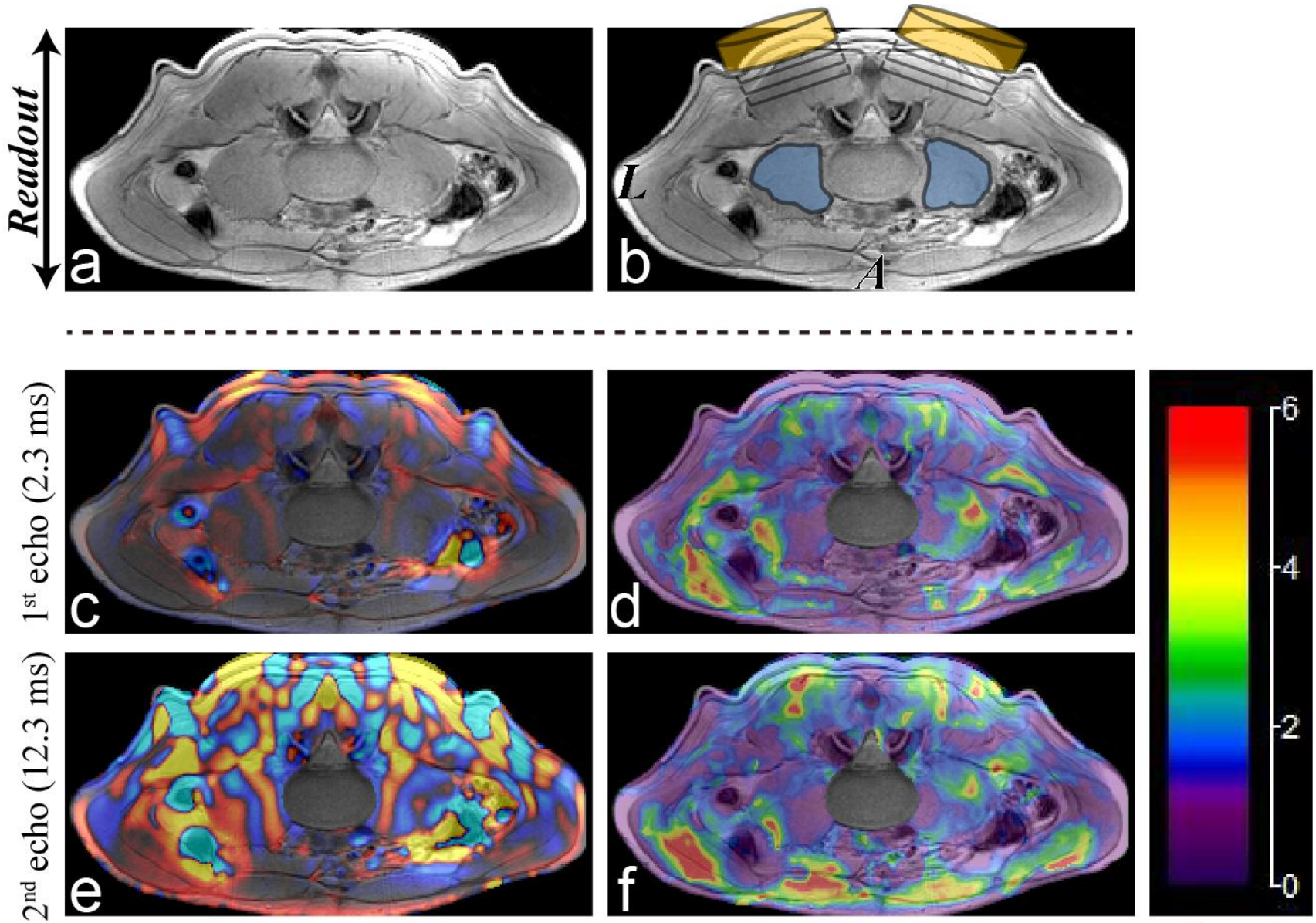
Readout
a
b
L
A
1st echo (2.3 ms)
c
d
2nd echo (12.3 ms)
e
f
6
4
2
0
Wave image fusion
Elastogram fusion
[kPa]

Fig.6